

Anomalous Thermal Transport Reveals Weak First-Order Melting of Charge Density Waves in 2H-TaSe₂

Authors: Han Huang^{1†}, Jinghang Dai^{1†}, Joyce Christiansen-Salameh¹, Jiyoung Kim¹, Samuel Kiehl¹, Desheng Ma², Noah Schinitzer^{3,4}, Danrui Ni⁵, Gustavo Alvarez¹, Chen Li¹, Carla Slebodnick⁶, Mario Medina¹, Bilal Azhar¹, Ahmet Alatas⁷, Robert Cava⁶, David Muller^{2,4}, Zhiting Tian^{1,*}

Affiliations:

¹Sibley School of Mechanical and Aerospace Engineering, Cornell University, Ithaca, New York 14853, USA

²School of Applied and Engineering Physics, Cornell University, Ithaca, NY 14853, USA

³Department of Materials Science and Engineering, Cornell University, Ithaca, NY 14853, USA

⁴Kavli Institute at Cornell for Nanoscale Science, Cornell University, Ithaca, NY 14853, USA

⁵Department of Chemistry, Princeton University, Princeton, New Jersey 08544, USA

⁶Department of Chemistry, Virginia Tech, Blacksburg, Virginia 24061, USA

⁷Advanced Photon Source, Argonne National Laboratory, Argonne, Illinois 60439, USA

†These two authors contribute equally

*Corresponding author. Email: zhiting@cornell.edu

Abstract: How ordered phases melt in low-dimensional quantum materials remain difficult to resolve because the relevant fluctuations are dynamic and charge neutral. In this work, we show that thermal transport provides a sensitive probe of these hidden fluctuations in the layered transition metal dichalcogenide 2H-TaSe₂. We observe a striking V-shaped temperature dependence of the thermal conductivity that cannot be explained by conventional phonon-phonon scattering. Instead, it originates from scattering by persistent local charge-density-wave (CDW) correlations, consistent with our phenomenological model linking thermal transport to spatial CDW fluctuation. Electron diffraction reveals short-range periodic lattice distortions persisting to at least 300 K, while X-ray diffraction shows thermal hysteresis of the CDW wavevector. Together, these results reveal a dislocation- and fluctuation-driven weak first-order melting of the CDW state.

INTRODUCTION

Phase transitions in low-dimensional systems exhibit a remarkable variety of behaviors that transcend the textbook dichotomy of discontinuous first-order and continuous second-order transitions. In two dimensions, thermal fluctuations can preclude conventional long-range order, giving rise instead to distinctive topological melting transitions, such as the Kosterlitz-Thouless-Halperin-Nelson-Young (KTHNY) framework (1, 2), where crystalline order vanishes through the continuous unbinding of dislocations and disclinations. Beyond these more common scenarios, theoretical studies have also proposed an intermediate regime in which discontinuous behavior and strong fluctuations may coexist (3, 4). Despite theoretical work, direct experimental access to this crossover regime remains challenging, largely because it requires a probe capable of simultaneously resolving microscopic defect dynamics, fluctuating local order, and macroscopic thermodynamic signatures that are charge neutral and span broad temperature ranges.

Layered transition metal dichalcogenides (TMDCs) provide an ideal platform for exploring phase transitions involving fluctuations and defects due to their reduced dimensionality and wide variety of ordered and fluctuating phases. Among them, 2H-TaSe₂ stands out as a canonical layered charge density wave (CDW) material. Upon cooling, it undergoes an incommensurate CDW transition at 122 K, followed by a commensurate transition at 90 K (5, 6). Despite decades of study using spectroscopic (7–13), transport (14–16), scattering (6, 7, 17–21), and real-space techniques (22, 23), key aspects of the CDW transition nature remain controversial. Several observations challenge traditional mechanisms involving Fermi surface nesting or saddle points: the metallic optical conductivity below the transition temperature (24), the large CDW gap (~ 0.1 eV) compared to $T_{CDW} = 122$ K (25, 26), and the short coherence length ($\xi^0 \sim 3 - 10$ Å) indicating strong fluctuations (27). Real-space transmission electron microscopy (TEM) studies of 2H-TaSe₂ crystals have also shown stripe-phase nucleation and dislocation-mediated evolution (22), suggesting that defects play an essential role microscopically in the CDW transition. These observations suggest that the CDW transition in 2H-TaSe₂ is governed by a complex interplay of fluctuations, defects, and lattice dynamics, which remain invisible to electronic or optical probes that do not couple directly to the charge-neutral lattice distortion. Consequently, probes capable of directly accessing these charge-neutral, lattice-coupled excitations and their dynamics are necessary.

While thermal conductivity measurements have been routinely performed as a measure of heat conduction, in this work, we demonstrate that thermal conductivity sensitively encodes the scattering signatures of the charge-neutral excitations and fluctuating order across complex phase transitions. Because phonons interact with virtually all excitations in a crystal, they are capable of sensing collective modes and hidden dynamics that are elusive conventional probes, thus making thermal conductivity measurement as a comprehensive diagnostic of these elusive degrees of freedom. Although thermal Hall conductivity has recently emerged as a specialized probe of Berry curvature and topological excitations (28), we demonstrate that longitudinal thermal transport possesses a more universal diagnostic reach. Its sensitivity to fluctuations and incipient order

especially facilitates the detection of subtle anomalies associated with exotic ordering phenomena. These features position thermal transport as a powerful and widely applicable probe for accessing elusive fluctuation physics in low-dimensional materials.

Our thermal transport measurements revealed a striking V-shaped temperature evolution of thermal conductivity featuring three distinct regimes: a pronounced peak near 122 K, a dip around 210 K, and an unexpected upturn at higher temperatures. This highly unusual behavior reflects strong scattering between heat carriers (phonons) and fluctuating local ordering, which occurs across a wide temperature range (up to 300 K), manifesting as topological defects. Complementary selected area electron diffraction (SAED) and X-ray diffraction (XRD) measurements reveal persistent short-range CDW order far above the long-range-order transition and thermal hysteresis in the CDW wavevector. Altogether, these results provide the first experimental discovery of a weak first-order CDW melting in a layered TMDC, demonstrating that the collective electronic-lattice correlations can persist far beyond their apparent stability range. To explain the anomalous thermal transport, we introduce a phenomenological model linking phonon-CDW scattering, order-parameter fluctuations, and anomalous thermal transport, successfully accounting for the high-temperature thermal conductivity recovery. These findings provide a new understanding of the phase boundaries and stability limits of correlated matter. We thereby establish thermal transport as a sensitive, nondestructive probe for phase transitions and emergent phenomena in layered materials involving complex coupled degrees of freedom. Intriguingly, our observation of fluctuating local CDW order suggests a fascinating parallel with cuprate high- T_c superconductors, which also host high-temperature fluctuating CDW phases (29, 30), pointing toward potentially universal features in the physics of low-dimensional quantum materials.

METHODS

2H-TaSe₂ has a hexagonal ($P6_3/mmc$) structure consisting of two layers of Se–Ta–Se sandwiches stacked along the c -axis, shown in **Fig. 1(a)**. Single crystals were synthesized via a two-step solid-state reaction followed by iodine-assisted chemical vapor transport in a temperature gradient of 1050–1000 °C for one week (31). The 2H phase was confirmed by single-crystal XRD (32–35). A microscope image of the measured sample is shown in **Fig. 1(b)**. IXS was performed at the Advanced Photon Source, Argonne National Laboratory (36, 37) to probe lattice dynamics along the [100] and [110] directions at 300 K, 115 K, and 80 K. The IXS data were fitted with the damped harmonic oscillation model to extract the phonon frequency and linewidth (32–35). XRD was performed at the Cornell High Energy Synchrotron Source (CHESS) from 80 K to 130 K with both cooling and warming cycles to detect thermal hysteresis. First-principles calculations using Temperature Dependent Effective Potentials (TDEP) (38, 39) with Vienna Ab Initio Simulation Package (VASP) (40, 41) were performed at room temperature to obtain finite temperature lattice dynamics (details in Supplementary Information (SI)).

In-plane thermal transport was measured using the transient thermal grating (TTG) technique, a non-contact optical pump–probe method illustrated in **Fig. 1(c)** (42–47) (details in SI). Exfoliated crystals were mounted on a coin-like copper holder with silver paste to ensure clean laser reflection

and good thermal contact at cryogenic temperatures. TTG data were fitted to extract the in-plane thermal diffusivity from 77 K to room temperature. (**Fig. S1**). Thermal conductivity from 78 K to 350 K was then obtained by combining the diffusivity with the specific heat estimated using the Debye model (48) (see **SI**), as shown in **Fig. S2**, and the density determined from XRD.

SAED measurements were performed on a mechanically exfoliated 2H-TaSe₂ flake transferred via polypropylene carbonate (PPC) stamp to a silicon nitride sample support. Diffraction patterns were collected on a Thermo Fisher Scientific Spectra 300 X-CFEG operated at 120 kV with a liquid nitrogen-cooled Gatan 636 specimen holder, and sample temperature was controlled with a Gatan 1905 heating controller.

RESULTS AND DISCUSSION

Guided by the premise that phonons couple broadly to lattice distortions, electronic ordering, and topological defects, we first examine the temperature dependence of the thermal conductivity across the CDW transition. As shown in **Fig. 2**, the normal phase (> 122 K) thermal conductivity exhibits a distinctive V-shaped temperature dependence. A sharp peak appears at $T_{CDW} = 122$ K, coinciding with the incommensurate to normal CDW transition. This peak originates from a λ -shaped specific heat peak at critical temperature driven by critical-like fluctuations of the CDW order, a hallmark of continuous phase transitions (SI). Upon warming, the thermal conductivity decreases until reaching a minimum around 210K. Most remarkably, above 210K, we observe an anomalous increase in thermal conductivity that persists to high temperatures, highly unusual for crystalline materials, where thermal conductivity typically decreases with increasing temperature due to enhanced phonon-phonon scattering. Meanwhile, the electronic contribution estimated from the Wiedemann-Franz law is small (around 5 W/m · K) (49) and does not account for the observed anomalous trend.

To assess whether changes in lattice dynamics alone can account for this behavior, we turn to IXS measurements. At 115 K, the IXS data reveal distinct low-energy modes near the CDW wave vector $\mathbf{q}_{CDW} \approx (0.33, 0, 0)$, at $q = 0.3$ and $q = 0.4$ along the $\Gamma - M$ direction (**Fig. 3**) compared to 300 K. No discernible phonon peak was observed at $q = 0.35$, likely because the signal is masked by strong elastic scattering when q is very close to \mathbf{q}_{CDW} . Comparison with prior IXS measurements from the same beamline (18) suggests that these modes arise from phonon softening. However, since these low-energy points disappear at 80 K, we do not rule out that they represent phase excitations specific to the incommensurate phase. The associated band bending near q_{CDW} results in a steep dispersion slope and higher phonon group velocity ($v_q = \partial_q \omega_q$), which may contribute to the conductivity enhancement near the transition (from 122 K to ~ 210 K). However, the enhanced phonon group velocity is confined to a narrow momentum region ($\delta|q| \sim 0.1$) (18), rendering it insufficient to account for the magnitude and breadth of the thermal conductivity change from 122 K to ~ 210 K. Also, this mechanism cannot account for the anomalous recovery of thermal conductivity observed at high temperatures above ~ 210 K. Moreover, the recovery of thermal conductivity above 210 K does not coincide with any known structural or electronic transition, indicating that conventional phonon-phonon scattering alone cannot explain the observed behavior, because upon warming, phonon-phonon scattering becomes stronger and suppresses thermal conductivity. Instead, these observations point to a competition between distinct phonon scattering channels, motivating consideration of unconventional scattering mechanisms associated with fluctuating order and defect-mediated lattice distortions at elevated temperatures.

To test this hypothesis, we examine how the underlying structural correlations evolve in the high-temperature regime. Our SAED measurements reveal distinctive residual CDW superlattice peaks persist even at 300K (**Fig. 4**), far above the long-range-order transition temperature of 122 K. These surviving satellite peaks demonstrates robust short-range (local) CDW order deep into the

nominally disordered phase. We also observe a linear increase in SAED peak widths with increasing temperature, as shown in **Fig. 4(e)**, suggesting a decreasing coherence length with $\frac{1}{|T-T_{CDW}|^\eta}$ scaling behavior, where $\eta \approx 1$. Notably, this scaling is valid not just a few Kelvins near the critical temperature but persists more than 150 K above T_{CDW} , underscoring the unusually long-lived nature of CDW correlations in this system. Importantly, the loss of CDW coherence manifests primarily through the suppression and broadening of discrete satellite peaks, rather than emerging into a ring-like diffuse scattering. The absence of pronounced azimuthal broadening suggests that the high-temperature CDW state does not correspond to a hexatic phase, as would be expected in a canonical KTHNY melting scenario, where orientational order is lost prior to translational order. Instead, in 2H-TaSe₂, the CDW wavevector remains locked to in-plane crystallographic directions even as translational coherence is progressively reduced. Previous XRD study on 2H-TaSe₂ also reported similar broad, nearly isotropic diffuse peaks persisting up to 200K (50). We attribute the absence of a diffuse ring to dimensionality and orientational pinning: in our bulk 2H-TaSe₂, interlayer coupling and lattice locking fix the CDW direction to in-plane crystallographic axes, suppressing the azimuthal averaging prominent in truly two-dimensional monolayers (e.g., 1T-TaS₂ (51)), thereby yielding fading lobes rather than a ring.

While SAED reveals the fluctuation-dominated character of the high-temperature phase, XRD provides a complementary thermodynamic perspective on the nature of the transition. Consistent with prior studies, our XRD also confirms the normal-to-incommensurate and incommensurate-to-commensurate CDW transitions at 122 K and 90 K, respectively, as shown in **Fig. 5**. Importantly, we observe clear thermal hysteresis of the CDW wavevector near the incommensurate transition temperature upon cooling and warming cycles, as shown in **Fig. 5(c)**. This hysteresis indicates latent energy associated with the transition, a defining feature of first-order transitions.

Taken together, the unconventional phonon scattering above T_{CDW} , the divergent specific heat at the critical point, the persistence of short-range CDW order far above T_{CDW} revealed by SAED, and the clear hysteresis of the CDW wavevector point to a weak first-order melting scenario for the CDW transition in 2H-TaSe₂, which has not been previously recognized in CDW systems. In this regime, the transition involves a subtle but finite discontinuity, manifested through latent energy and phase coexistence, while remaining strongly influenced by fluctuations and defect proliferation and giving rise to an extended temperature range of short-range order. This behavior is fundamentally distinct from both conventional first-order transitions, which exhibit abrupt loss of order with minimal precursor fluctuations, and continuous KTHNY-type melting (1, 2), where topological defect unbinding proceeds without thermodynamic hysteresis. This interpretation also aligns with contemporary theoretical frameworks for phase transitions in general 2D and quasi-2D systems, which allow for multiple melting scenarios depending on specific material parameters and interaction potentials (3, 4, 52–54). Notably, related 2D CDW materials such as 1T-TaS₂ also exhibit persistent local CDW order well above their transition temperatures (51, 55, 56), suggesting that dislocation- and fluctuation-driven melting may represent a unifying description for CDW transitions in low-dimensional layered materials, but the melting in 1T-TaS₂ is of

KTHNY type involving a hexatic process. Our results also argue against the Ising-type transition model proposed by Gor'kov (57), in which Ta atoms hop between two potential minima in analogy with spin flips due to strong electron-phonon coupling. In this Ising scenario, the transition is strictly second order at T_{CDW} . While strong electron-phonon coupling remains central to the ordered CDW phase, evidenced by phonon softening, the transition itself proceeds through a melting-like evolution characterized by continuous spectral broadening and q-vector hysteresis.

The persistent short-range CDW order above T_{CDW} provides a natural explanation for the anomalous thermal conductivity. As temperature increases through T_{CDW} , the long-range CDW order gradually melts into short-range correlations, as shown by the reduced coherence length and persistent satellite peaks in SAED. In this intermediate regime, growing spatial fluctuations enhance phonon-CDW scattering, leading to suppressed thermal conductivity. Meanwhile, as the temperature increases, the local CDW domains become increasingly short-ranged and dilute, resulting in fewer phonon-CDW scattering events. This competition between these two effects explains the unusual V-shaped temperature dependence observed in our thermal conductivity measurements, with a minimum around 210K separating the two competing regimes.

This picture can be formalized by modeling phonon scattering from spatial fluctuations of the CDW order parameter (full details in SI), expressed as $\psi(r)a = A(r) \exp[iq(z + u(r))]$, where $A(r)$ is the CDW amplitude and $u(r)$ represents wavefront distortions. The spatial gradient of the order parameter ($\nabla\psi(r)$) quantifies disorder caused by elastic deformations and dislocations. Within the Born approximation, the scattering rate is proportional to the variance of these gradients, given by

$$\tau_{CDW}^{-1}(T) \propto \langle |\nabla A|^2 \rangle + q^2 \langle A^2 (\nabla u)^2 \rangle. \quad (1)$$

Experimentally, the CDW diffraction peak width $w(T)$ reflects $\langle (\nabla u)^2 \rangle$, while the integrated peak intensity tracks $A^2(T)$. Thus, we can show that the CDW contribution to the scattering rate can be expressed phenomenologically as

$$\tau_{CDW}^{-1}(T) = aw(T)^2 A^2(T), \quad (2)$$

with a being a material-dependent constant. The total thermal conductivity is then obtained from kinetic theory as $\kappa(T) = \frac{1}{3} C_v(T) v_s^2 \tau_{tot}(T)$, where v_s is the sound velocity and $C_{v(T)}$ is the phonon specific heat per unit volume. The scattering rate is given by a Matthiessen sum

$$\tau_{tot}^{-1}(T) = A_U T \exp\left(-\frac{\theta_U}{T}\right) + A_{imp} + \tau_{CDW}^{-1}(T) \quad (3)$$

where A_U and θ_U parametrize Umklapp scattering, and A_{imp} accounts for impurity scattering. The specific heat is described by the Debye model with $\theta_D = 200$ K. The peak width is fitted as $w(T) = w^0 + m(T - 100K)$, where the fitted $w_0 \approx 0.0865 \text{ \AA}^{-1}$ and $m \approx 0.00168 \text{ \AA}^{-1} K^{-1}$. The amplitude softening is modelled as a logistic decay $A^2(T) = \left[1 + \exp\left(\frac{T - T^0}{\Delta}\right)\right]^{-s}$, where T^0 , Δ , and s are fitting parameters. Fitting to experimental thermal conductivity data results in $A_U =$

$1.316 \times 10^5 \text{ s}^{-1}\text{K}^{-1}$, $A_{imp} = 4.758 \times 10^6 \text{ s}^{-1}$, $a_{CDW} = 5.327 \times 10^8 \text{ s}^{-1} \text{ \AA}^2$, $\Theta_U = 120\text{K}$, $T^0 = 196.88\text{K}$, $\Delta = 3.95\text{K}$, and $s \sim 0.122$. The fitted curve is shown in **Fig. 2**. This formulation captures the measured V-shaped behavior of $\kappa(T)$, since CDW scattering rates grow with $w^2 A^2$ at intermediate temperatures ($122\text{K} \sim 210\text{K}$), driving a minimum in thermal conductivity, and diminish once the amplitude collapses, allowing $\kappa(T)$ to recover at elevated temperatures.

Finally, we note that the thermal conductivity values obtained here using TTG are systematically higher than those reported in earlier steady-state measurements (50). We attribute this discrepancy to sample quality variations, where different impurity concentrations can strongly influence CDW pinning and thus phonon scattering, as previously observed in related materials such as 2H-NbS₂ (58). Increased impurity pinning strongly stabilizes local CDW regions and enhances phonon scattering, reducing thermal conductivity. This sensitivity to impurities also explains the wide variation in reported properties across different studies (23, 59, 60), further emphasizing the importance of high-quality samples for accurate characterization of the intrinsic behaviors.

The implications of our findings extend beyond the fundamental understanding of CDW transitions, offering new insight into the phase boundaries and stability limits of correlated matters. The persistence of local CDW order far above the long-range transition temperature indicates that CDW-related phenomena, such as enhanced electron–phonon coupling and modified electronic structure, can remain active well into the nominally normal phase. This observation suggests that conventional phase diagrams, defined solely by the disappearance of long-range order, may underestimate the temperature range over which CDW correlations influence material properties. This behavior is also relevant to other correlated systems, particularly high-temperature superconductors, where short-range charge ordering and fluctuating electronic correlations persist in the pseudogap regime well above the superconducting transition temperature. Our results therefore provide a model example of how fluctuating charge order can influence electronic structure and transport without long-range order. More broadly, our results highlight how the interplay among lattice distortions, electronic instabilities, and defect-mediated spatial heterogeneity can govern both thermal transport and ordering phenomena in low-dimensional quantum materials, and further demonstrate that thermal transport measurements provide a powerful probe of hidden fluctuating order, offering a complementary pathway to investigate pseudogap-like regimes and intertwined orders in a wide range of correlated materials.

References and Notes

1. J. M. Kosterlitz, D. J. Thouless, Ordering, metastability and phase transitions in two-dimensional systems. *Journal of Physics C: Solid State Physics* **6**, 1181–1203 (1973).
2. B. I. Halperin, D. R. Nelson, Theory of Two-Dimensional Melting. *Physical Review Letters* **41**, 121–124 (1978).
3. Y. Kato, N. Nagaosa, Monte Carlo simulation of two-dimensional flux-line-lattice melting. *Physical Review B* **48**, 7383–7391 (1993).
4. J. Hu, A. H. MacDonald, Two-dimensional vortex lattice melting. *Physical Review Letters* **71**, 432–435 (1993).
5. J. A. Wilson, F. J. Di Salvo, S. Mahajan, Charge-density waves and superlattices in the metallic layered transition metal dichalcogenides. *Advances in Physics* **24**, 117–201 (1975).
6. D. E. Moncton, J. D. Axe, F. J. DiSalvo, Neutron scattering study of the charge-density wave transitions in 2H-TaSe_2 and 2H-NbSe_2 . *Phys. Rev. B* **16**, 801–819 (1977).
7. J. Laverock, D. Newby, E. Abreu, R. Averitt, K. E. Smith, R. P. Singh, G. Balakrishnan, J. Adell, T. Balasubramanian, k -resolved susceptibility function of 2H-TaSe_2 from angle-resolved photoemission. *Phys. Rev. B* **88**, 035108 (2013).
8. D. S. Inosov, V. B. Zabolotnyy, D. V. Evtushinsky, A. A. Kordyuk, B. Büchner, R. Follath, H. Berger, S. V. Borisenko, Fermi surface nesting in several transition metal dichalcogenides. *New Journal of Physics* **10**, 125027 (2008).
9. S. V. Borisenko, A. A. Kordyuk, A. N. Yaresko, V. B. Zabolotnyy, D. S. Inosov, R. Schuster, B. Büchner, R. Weber, R. Follath, L. Patthey, H. Berger, Pseudogap and Charge Density Waves in Two Dimensions. *Physical Review Letters* **100**, 196402 (2008).
10. T. Valla, A. V. Fedorov, P. D. Johnson, J. Xue, K. E. Smith, F. J. DiSalvo, Charge-Density-Wave-Induced Modifications to the Quasiparticle Self-Energy in 2H-TaSe_2 . *Phys. Rev. Lett.* **85**, 4759–4762 (2000).
11. Y. W. Li, J. Jiang, H. F. Yang, D. Prabhakaran, Z. K. Liu, L. X. Yang, Y. L. Chen, Folded superstructure and degeneracy-enhanced band gap in the weak-coupling charge density wave system 2H-TaSe_2 . *Phys. Rev. B* **97**, 115118 (2018).
12. D. V. Evtushinsky, A. A. Kordyuk, V. B. Zabolotnyy, D. S. Inosov, B. Büchner, H. Berger, L. Patthey, R. Follath, S. V. Borisenko, Pseudogap-Driven Sign Reversal of the Hall Effect. *Physical Review Letters* **100**, 236402 (2008).
13. M. Li, N. Xu, J. Zhang, R. Lou, M. Shi, L. Li, H. Lei, C. Petrovic, Z. Liu, K. Liu, Y. Huang, S. Wang, Quantization of the band at the surface of charge density wave material 2H-TaSe_2 . *Chinese Physics B* **30**, 047305 (2021).

14. J. Demsar, L. Forró, H. Berger, D. Mihailovic, Femtosecond snapshots of gap-forming charge-density-wave correlations in quasi-two-dimensional dichalcogenides 1T-TaS₂ and 2H-TaSe₂. *Physical Review B - Condensed Matter and Materials Physics* **66**, 411011–411014 (2002).
15. B. Ruzicka, L. Degiorgi, H. Berger, R. Gaál, L. Forró, Charge dynamics of 2H-TaSe₂ along the less-conducting c-axis. *Physical Review Letters* **86**, 4136–4139 (2001).
16. V. Vescoli, L. Degiorgi, H. Berger, L. Forró, Dynamics of Correlated Two-Dimensional Materials: The 2H-TaSe₂ Case. *Phys. Rev. Lett.* **81**, 453–456 (1998).
17. E. F. Steigmeier, G. Harbeke, H. Auderset, F. J. DiSalvo, Softening of charge density wave excitations at the superstructure transition in 2H-TaSe₂. *Solid State Communications* **20**, 667–671 (1976).
18. X. Shen, R. Heid, R. Hott, A.-A. Haghighirad, B. Salzmann, M. dos Reis Cantarino, C. Monney, A. H. Said, M. Frachet, B. Murphy, K. Rossnagel, S. Rosenkranz, F. Weber, Precursor region with full phonon softening above the charge-density-wave phase transition in 2H-TaSe₂. *Nature Communications* **14**, 7282 (2023).
19. R. L. Barnett, A. Polkovnikov, E. Demler, W. G. Yin, W. Ku, Coexistence of gapless excitations and commensurate charge-density wave in the 2H transition metal dichalcogenides. *Physical Review Letters* **96** (2006).
20. Y. Ge, A. Y. Liu, Effect of dimensionality and spin-orbit coupling on charge-density-wave transition in 2H-TaSe₂. *Physical Review B - Condensed Matter and Materials Physics* **86** (2012).
21. S. Chowdhury, A. F. Rigosi, H. M. Hill, A. Briggs, D. B. Newell, H. Berger, A. R. Hight Walker, F. Tavazza, Influence of Dimensionality on the Charge Density Wave Phase of 2H-TaSe₂. *Advanced Theory and Simulations* **5** (2022).
22. C. H. Chen, J. M. Gibson, R. M. Fleming, Microstructure in the incommensurate and the commensurate charge-density-wave states of 2H-TaSe₂: A direct observation by electron microscopy. *Physical Review B* **26**, 184–205 (1982).
23. Z. Zhang, C. Xie, M. Hong, J. Shi, S. Pan, J. Hu, Q. Wu, W. Quan, N. Gao, J. Zhao, Y. Zhang, Scanning Tunneling Microscopy Examinations of the Effects of Defects on the Charge Density Wave Order in the Chemical Vapor Deposition-Derived TaSe₂ on Au Foils. *Journal of Physical Chemistry C* **127**, 16560–16566 (2023).
24. S. V. Dordevic, D. N. Basov, R. C. Dynes, B. Ruzicka, V. Vescoli, L. Degiorgi, H. Berger, R. Gaál, L. Forró, E. Bucher, Optical properties of the quasi-two-dimensional dichalcogenides 2H-TaSe₂ and 2H-NbSe₂. *European Physical Journal B* **33**, 15–23 (2003).
25. A. S. Barker, J. A. Ditzenberger, F. J. DiSalvo, Infrared study of the electronic instabilities in tantalum disulfide and tantalum diselenide. *Physical Review B* **12**, 2049–2054 (1975).

26. R. V. Coleman, B. Giambattista, P. K. Hansma, A. Johnson, W. W. McNairy, C. G. Slough, Scanning tunnelling microscopy of charge-density waves in transition metal chalcogenides. *Advances in Physics* **37**, 559–644 (1988).
27. W. L. McMillan, Microscopic model of charge-density waves in 2H-TaSe₂. *Physical Review B* **16**, 643–650 (1977).
28. M. Li, G. Chen, Thermal transport for probing quantum materials. *MRS Bulletin* **45**, 348–356 (2020).
29. R. Arpaia, S. Caprara, R. Fumagalli, G. De Vecchi, Y. Y. Peng, E. Andersson, D. Betto, G. M. De Luca, N. B. Brookes, F. Lombardi, M. Salluzzo, L. Braicovich, C. Di Castro, M. Grilli, G. Ghiringhelli, Dynamical charge density fluctuations pervading the phase diagram of a Cu-based high- T_c superconductor. *Science* **365**, 906–910 (2019).
30. D. H. Torchinsky, F. Mahmood, A. T. Bollinger, I. Božović, N. Gedik, Fluctuating charge-density waves in a cuprate superconductor. *Nature Materials* **12**, 387–391 (2013).
31. H. Luo, W. Xie, J. Tao, H. Inoue, A. Gyenis, J. W. Krizan, A. Yazdani, Y. Zhu, R. J. Cava, Polytypism, polymorphism, and superconductivity in TaSe_{2-x}Te_x. *Proceedings of the National Academy of Sciences* **112** (2015).
32. H. Ma, C. Li, Y. Ma, H. Wang, Z. W. Rouse, Z. Zhang, C. Slebodnick, A. Alatas, S. P. Baker, J. J. Urban, Z. Tian, Supercompliant and Soft (CH₃NH₃)₃Bi₂I₉ Crystal with Ultralow Thermal Conductivity. *Physical Review Letters* **123** (2019).
33. H. Ma, Y. Ma, H. Wang, C. Slebodnick, A. Alatas, J. J. Urban, Z. Tian, Experimental Phonon Dispersion and Lifetimes of Tetragonal CH₃NH₃PbI₃ Perovskite Crystals. *Journal of Physical Chemistry Letters* **10**, 1–6 (2019).
34. H. Ma, C. Li, S. Tang, J. Yan, A. Alatas, L. Lindsay, B. C. Sales, Z. Tian, Boron arsenide phonon dispersion from inelastic x-ray scattering: Potential for ultrahigh thermal conductivity. *Physical Review B* **94**, 220303 (2016).
35. Z. T. Tian, M. D. Li, Z. S. Ren, H. Ma, A. Alatas, S. D. Wilson, J. Li, Inelastic x-ray scattering measurements of phonon dispersion and lifetimes in PbTe_{1-x}Se_x alloys. *Journal of Physics: Condensed Matter* **27**, 375403 (2015).
36. A. H. Said, H. Sinn, T. S. Toellner, E. E. Alp, T. Gog, B. M. Leu, S. Bean, A. Alatas, High-energy-resolution inelastic X-ray scattering spectrometer at beamline 30-ID of the Advanced Photon Source. *Journal of Synchrotron Radiation* **27**, 827–835 (2020).
37. T. S. Toellner, A. Alatas, A. H. Said, Six-reflection meV-monochromator for synchrotron radiation. *Journal of Synchrotron Radiation* **18**, 605–611 (2011).
38. O. Hellman, P. Steneteg, I. A. Abrikosov, S. I. Simak, Temperature dependent effective potential method for accurate free energy calculations of solids. *Physical Review B - Condensed Matter and Materials Physics* **87** (2013).

39. O. Hellman, I. A. Abrikosov, S. I. Simak, Lattice dynamics of anharmonic solids from first principles. *Physical Review B* **84**, 180301 (2011).
40. G. Kresse, J. Furthmüller, Efficient iterative schemes for *ab initio* total-energy calculations using a plane-wave basis set. *Physical Review B* **54**, 11169–11186 (1996).
41. G. Kresse, J. Hafner, *Ab initio* molecular dynamics for liquid metals. *Physical Review B* **47**, 558–561 (1993).
42. C. Li, H. Ma, T. Li, J. Dai, Md. A. J. Rasel, A. Mattoni, A. Alatas, M. G. Thomas, Z. W. Rouse, A. Shragai, S. P. Baker, B. J. Ramshaw, J. P. Feser, D. B. Mitzi, Z. Tian, Remarkably Weak Anisotropy in Thermal Conductivity of Two-Dimensional Hybrid Perovskite Butylammonium Lead Iodide Crystals. *Nano Lett.* **21**, 3708–3714 (2021).
43. B. S. Chang, C. Li, J. Dai, K. Evans, J. Huang, M. He, W. Hu, Z. Tian, T. Xu, Thermal Percolation in Well-Defined Nanocomposite Thin Films. *ACS Appl. Mater. Interfaces* **14**, 14579–14587 (2022).
44. C. Li, Y. Ma, Z. Tian, Thermal Switching of Thermoresponsive Polymer Aqueous Solutions. *ACS Macro Letters* **7** (2018).
45. J. Dai, Q. Fang, G. A. Alvarez, A. Schaeffer, K. A. Page, J. Kim, S. M. Kielar, J. Christiansen-Salameh, E. Jeong, D. D. Bhagwandin, J. Kwon, L. D. Tran, M. S. Islam, A. K. Roy, N. R. Glavin, Y. Zhong, J. Lou, Z. Tian, Directly measured high in-plane thermal conductivity of two-dimensional covalent organic frameworks. *Nature Communications* **16** (2025).
46. J. Dai, S. Kielar, J. Kim, R. J. Warzoha, C. Li, M. Medina, B. Azhar, Z. Tian, Directly Probing Thermal Transport Across Micrometer-Thick Metallic Interfaces Using Transient Thermal Grating Spectroscopy. *Small Methods* **10** (2026).
47. X. Zhang, J. Dai, C. Li, H. Ma, Characterizing thermal energy materials using transient grating spectroscopy: A comprehensive review of principles, techniques, and applications. *Journal of Laser Applications* **37** (2025).
48. J. M. E. Harper, T. H. Geballe, F. J. DiSalvo, Thermal properties of layered transition-metal dichalcogenides at charge-density-wave transitions. *Physical Review B* **15**, 2943–2951 (1977).
49. T. Kumakura, H. Tan, T. Handa, M. Morishita, H. Fukuyama, Charge density waves and superconductivity in 2H-TaSe₂. *Czechoslovak Journal of Physics* **46**, 2611–2612 (1996).
50. M. D. Nunez-Regueiro, J. M. Lopez-Castillo, C. Ayache, “Thermal Conductivity of 1 T-TaS₂ and 2H-TaSe₂” (1985).
51. J. M. Shen, A. Stangel, S. H. Sung, I. E. Baggari, K. Sun, R. Hovden, Melting of Charge Density Waves in Low Dimensions. arXiv [Preprint] (2025).
<https://doi.org/10.48550/ARXIV.2505.07569>.

52. V. N. Ryzhov, E. E. Tareyeva, Y. D. Fomin, E. N. Tsiok, Berezinskii—Kosterlitz—Thouless transition and two-dimensional melting. *Uspekhi Fizicheskikh Nauk* **187**, 921–951 (2017).
53. E. P. Bernard, W. Krauth, Two-step melting in two dimensions: First-order liquid-hexatic transition. *Physical Review Letters* **107** (2011).
54. B. I. Halperin, T. C. Lubensky, S. Ma, First-Order Phase Transitions in Superconductors and Smectic- A Liquid Crystals. *Phys. Rev. Lett.* **32**, 292–295 (1974).
55. J. Joshi, H. M. Hill, S. Chowdhury, C. D. Malliakas, F. Tavazza, U. Chatterjee, A. R. Hight Walker, P. M. Vora, Short-range charge density wave order in 2H- T a S2. *Physical Review B* **99** (2019).
56. S. H. Sung, N. Agarwal, I. El Baggari, P. Kezer, Y. M. Goh, N. Schnitzer, J. M. Shen, T. Chiang, Y. Liu, W. Lu, Y. Sun, L. F. Kourkoutis, J. T. Heron, K. Sun, R. Hovden, Endotaxial stabilization of 2D charge density waves with long-range order. *Nature Communications* **15**, 1403 (2024).
57. L. P. Gor'kov, Strong electron-lattice coupling as the mechanism behind charge density wave transformations in transition-metal dichalcogenides. *Physical Review B - Condensed Matter and Materials Physics* **85** (2012).
58. C. Wen, Y. Xie, Y. Wu, S. Shen, P. Kong, H. Lian, J. Li, H. Xing, S. Yan, Impurity-pinned incommensurate charge density wave and local phonon excitations in 2H-NbS2. *Physical Review B* **101** (2020).
59. H. Ryu, Y. Chen, H. Kim, H. Z. Tsai, S. Tang, J. Jiang, F. Liou, S. Kahn, C. Jia, A. A. Omrani, J. H. Shim, Z. Hussain, Z. X. Shen, K. Kim, B. I. Min, C. Hwang, M. F. Crommie, S. K. Mo, Persistent Charge-Density-Wave Order in Single-Layer TaSe2. *Nano Letters* **18**, 689–694 (2018).
60. M. Lee, M. Šiškins, S. Mañas-Valero, E. Coronado, P. G. Steeneken, H. S. J. van der Zant, Study of charge density waves in suspended 2H-TaS2 and 2H-TaSe2 by nanomechanical resonance. *Applied Physics Letters* **118** (2021).
61. H. Huang, J. Dai, J. Christiansen-Salameh, J. Kim, S. Kielar, D. Ma, N. Schinitzer, D. Ni, G. Alvarez, C. Li, C. Slednick, M. Medina, B. Azhar, A. Alatas, R. Cava, D. Muller, Z. Tian, Dataset: Anomalous Thermal Transport Reveals Weak First-Order Melting of Charge Density Waves in 2H-TaSe2, *PARADIM* (2026).
62. R. Huisman, F. Jellinek, On the polymorphism of tantalum diselenide. *Journal of the Less Common Metals* **17**, 111–117 (1969).
63. J. P. Perdew, K. Burke, M. Ernzerhof, Generalized Gradient Approximation Made Simple. *Physical Review Letters* **77**, 3865–3868 (1996).
64. P. M. Chaikin, T. C. Lubensky, *Principles of Condensed Matter Physics* (Cambridge University Press, 1995).

Acknowledgments: HH, JD, and ZT thank Allan MacDonald for fruitful discussions and suggestions. HH, JD, JC, GA, and ZT thank Jacob Ruff for assistance with X-ray diffraction measurements and helpful discussions. DM and NS thank Saif Siddique for assistance with the preparation of exfoliated samples for TEM analysis. This research used resources of the Advanced Photon Source, a U.S. Department of Energy (DOE) Office of Science user facility operated for the DOE Office of Science by Argonne National Laboratory under Contract No. DE-AC02-06CH11357. Research conducted at the Center for High-Energy X-ray Sciences (CHEXS) was supported by the National Science Foundation (BIO, ENG and MPS Directorates) under awards DMR-1829070 and DMR-2342336. This research made use of the electron microscopy facility of the Platform for the Accelerated Realization, Analysis, and Discovery of Interface Materials (PARADIM), which is supported by the National Science Foundation under Cooperative Agreement No. DMR-2039380 and the Cornell Center for Materials Research shared instrumentation facility. The Thermo Fisher Spectra 300 X-CFEG was acquired with support from PARADIM, an NSF MIP (DMR-2039380), and Cornell University. CS thanks the NSF under 1726077 for the single-crystal X-ray diffraction experiments.

Funding:

Office of Naval Research award N00014-22-1-2357 (HH, JD, ZT)

National Science Foundation awards DMR-1829070 supporting the Center for High-Energy X-ray Sciences (CHEXS)

National Science Foundation awards DMR-2342336 supporting the Center for High-Energy X-ray Sciences (CHEXS)

National Science Foundation Cooperative Agreement DMR-2039380 supporting the Platform for the Accelerated Realization, Analysis, and Discovery of Interface Materials (PARADIM)

National Science Foundation grant 1726077 supporting single-crystal X-ray diffraction experiments (CS)

U.S. Department of Energy Office of Science user facility support for the APS under Contract No. DE-AC02-06CH11357

Author contributions:

Conceptualization: HH, JD, ZT

Methodology: HH, JD, DMa, AA, DMu, ZT

Investigation: HH, JD, JC, JK, SK, DMa, NS, GA, CL, CS, MM, BA, AA

Data Curation: HH, JD, JC, DMa, NS, CS, MM, CL

Formal Analysis: HH, JD, JC, MM

Visualization: HH, JD, JC, MM, CS

Funding acquisition: CS, DMu, ZT

Project administration: HH, JD, ZT

Resources: ZT, DN, RC

Supervision: ZT

Writing – original draft: HH, JD, ZT

Writing – review & editing: HH, JD, JC, DMa, NS, CS, AA, RC, DMu,

Competing interests: The authors declare no competing interests.

Data, code, and materials availability:

The electron microscopy datasets in this study are available through PARADIM (61), a National Science Foundation Materials Innovation Platform. All other raw data supporting the findings of this study are available upon request.

Supplementary Materials

Materials and Methods

Supplementary Text

Figs. S1 to S7

Tables S1 to S2

References (62–64)

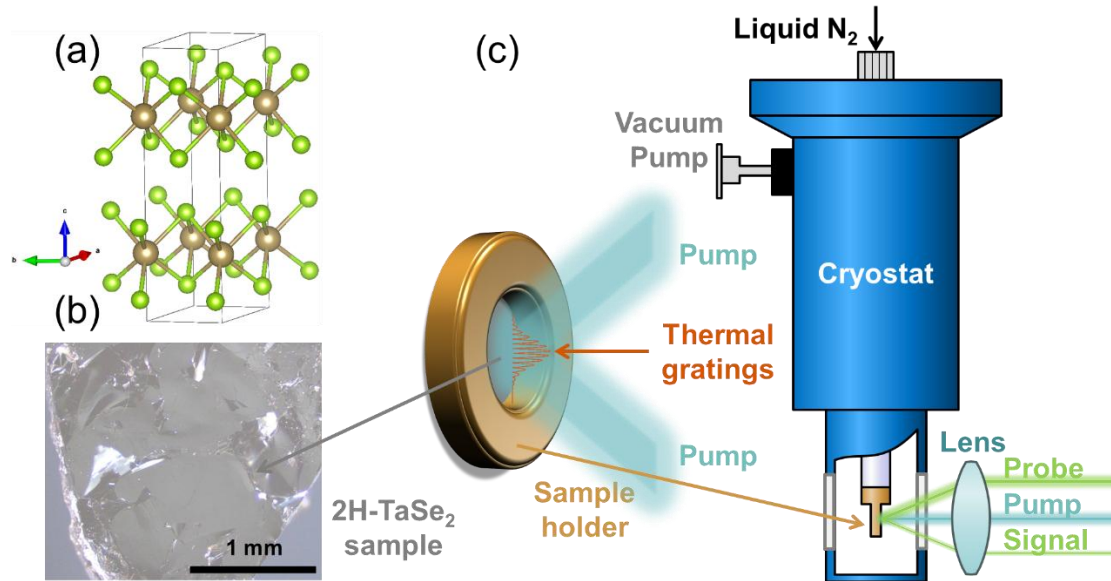


Fig. 1. (a) The unit cell structure of 2H-TaSe₂; (b) The microscope photo of an exfoliated 2H-TaSe₂ sample ready to be put inside a cryostat and measured. The scale bar is 1 mm; (c) The illustration of a laser-based transient thermal grating (TTG) setup with the sample mounted inside the cryostat. The exfoliated 2H-TaSe₂ sample in (b) was mounted on a copper holder, which was loaded into the cryostat and placed under vacuum. Liquid N₂ and a heater are used to stabilize the sample temperature via a PID controller. Two pulsed pump lasers are crossed at the sample surface, and a sinusoidal temperature distribution is formed at the crossed region. The continuous wave probe laser detects the decay of the sinusoidal temperature distribution in a reflection geometry of TTG.

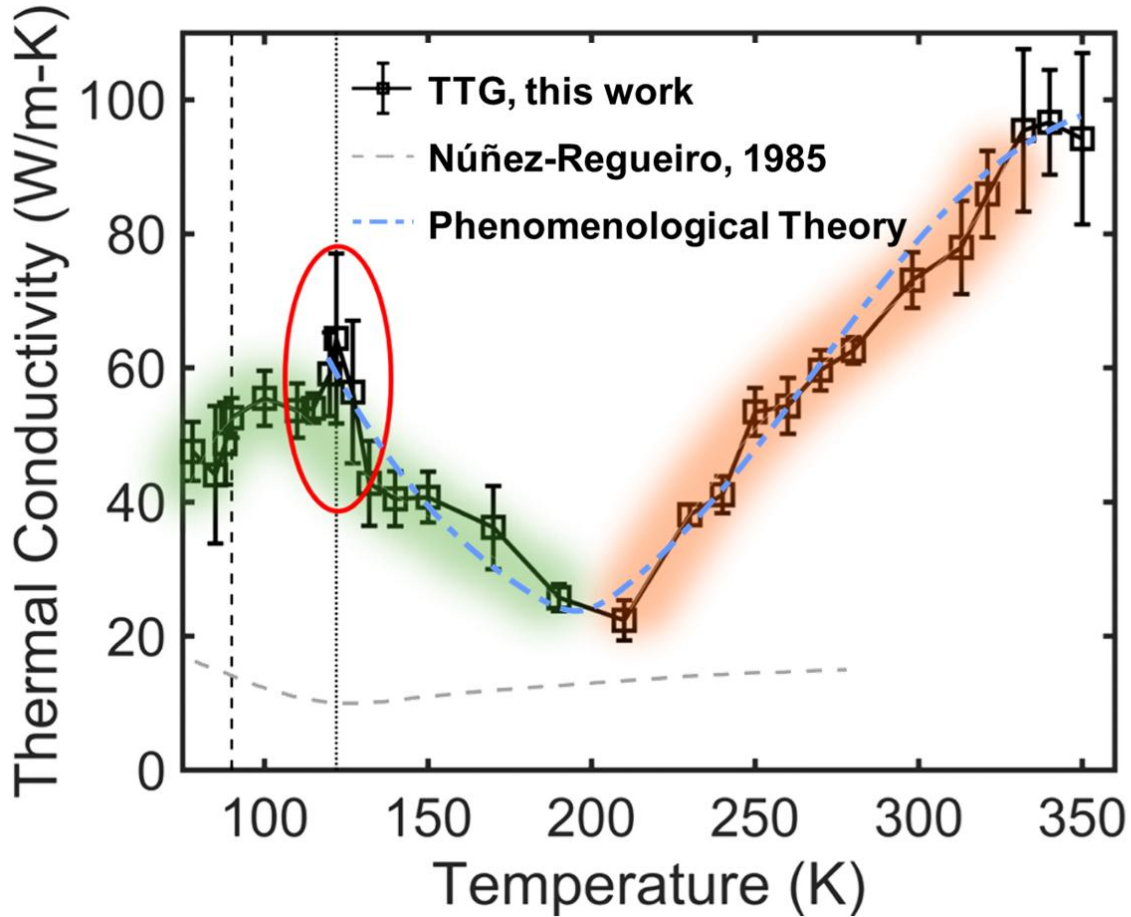


Fig. 2. Temperature-dependent thermal conductivity of 2H-TaSe₂ from 78 K to 350 K. The two transition temperatures are marked as a vertical dash (90 K) and a dotted line (122 K). The red circle highlights a pronounced peak in the thermal conductivity resulting from a λ -shaped peak in specific heat capacity, reflecting a strong enhancement of the specific heat associated with critical-like fluctuations near the transition, a behavior characteristic of continuous phase transitions and suggestive of a weak first-order crossover regime. The green and orange shades mark the regions on either side of the 210 K dip within the V-shaped trend. The blue dotted dash curve is fitted using our phenomenological formula. The measurement from previous work (50) is plotted for comparison.

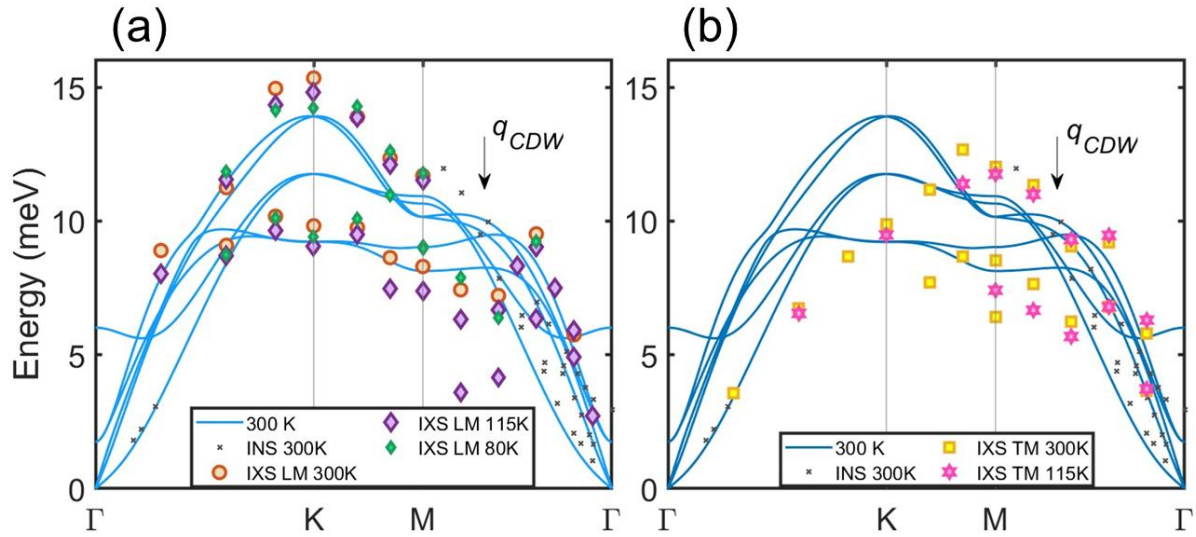


Fig. 3. Phonon dispersion of 2H-TaSe₂: the blue lines are from TDEP first principles calculation; the black dots are the room temperature inelastic neutron scattering (INS) measurement from literature (\diamond). For (a), the red circles are IXS measured longitudinal phonon modes at room temperature; the purple diamonds are IXS measured longitudinal phonon modes at 115 K; the purple diamonds are IXS measured longitudinal phonon modes at 80 K. For (b), the yellow squares are IXS measured transverse phonon modes at room temperature; the pink stars are IXS measured transverse phonon modes at 115 K.

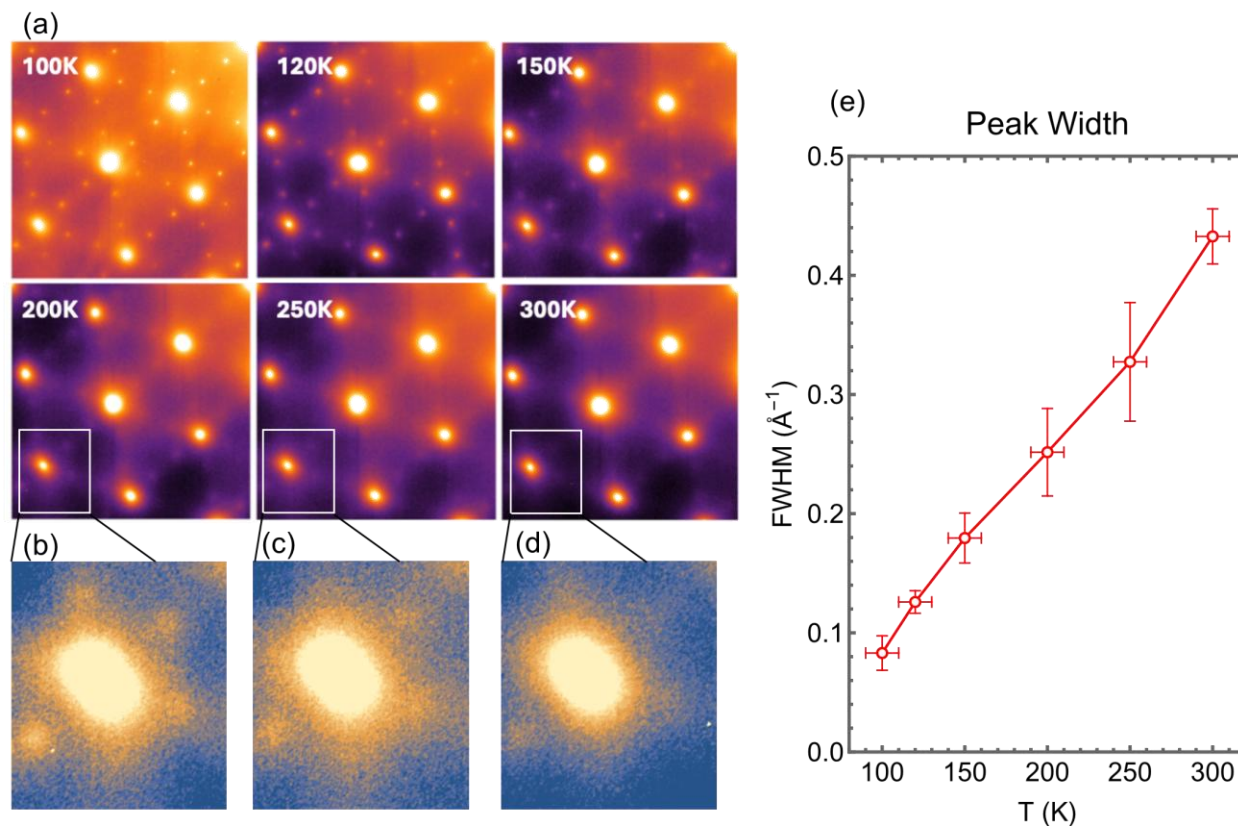


Fig. 4 (a) Temperature-dependent electron diffraction showing Bragg peaks and CDW superlattice at 100K, 120K, 150K, 200K, 250K, and 300K; (b)-(d) zoom-in figure of filtered-out residue peaks at 200K, 250K, and 300K, indicating residue local CDW order at high temperatures; (e) superlattice peak widths from electron diffraction, which increase as temperature increases, indicating diminishing local CDW order. The horizontal temperature error bar comes from the spatial separation between the holder-mounted temperature sensor and the sample position, which introduces uncertainty in the actual sample temperature for each SAED dataset.

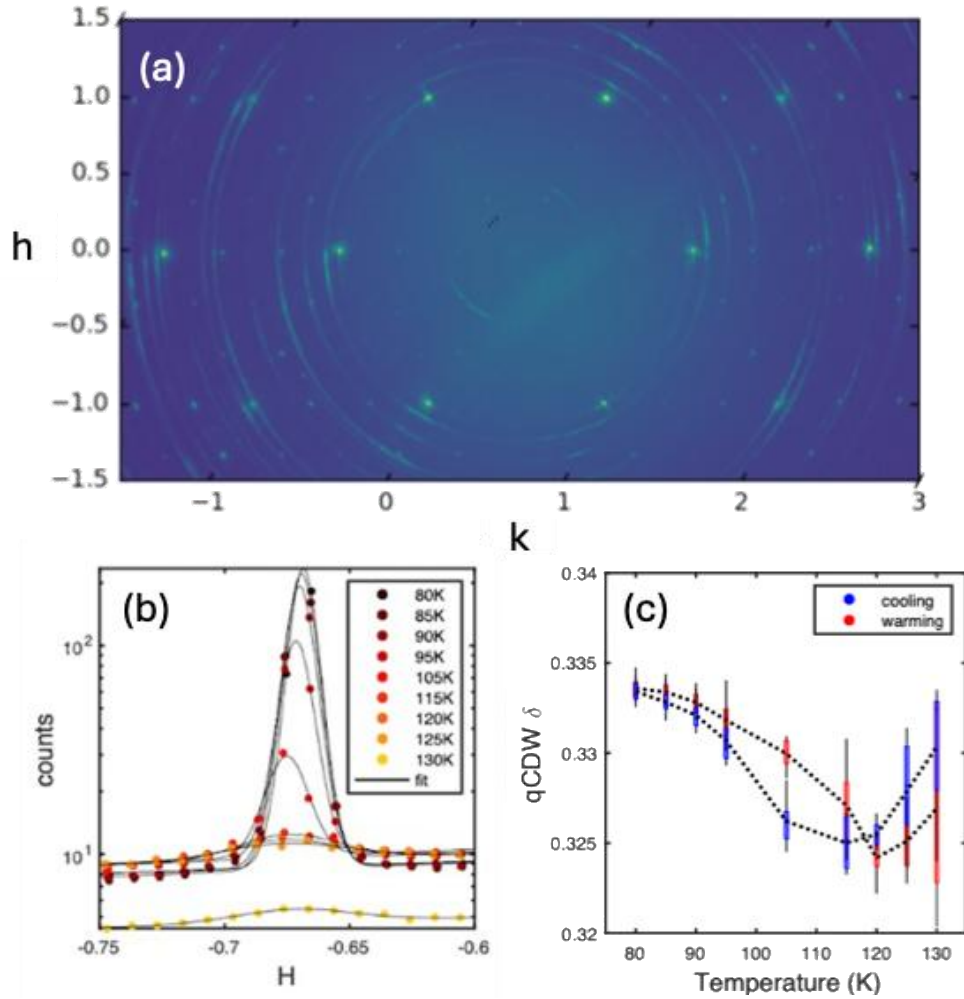


Fig. 5 (a) X-ray scattering data taken at 80 K of the $hk0$ plane, clean diffraction peaks indicated good crystalline order in the hexagonal plane; (b) Cooling data collected at the $(001) - (1/3 + \delta, 0, 0)$ superlattice reflection, where representative line scans at each temperature were fitted with Gaussian profiles to extract the peak position and integrated intensity, and each reported peak position was obtained by averaging over more than 30 symmetry-equivalent superlattice peaks within the same diffraction pattern, with error bars representing the statistical uncertainty of this averaging; (c) Thermal hysteresis of $|q_{CDW}|$, indicating latent heat associated with first-order transition.